The Coupling of Electron Transfer and Proton Translocation: Electrostatic Calculations on *Paracoccus denitrificans* Cytochrome *c* Oxidase

Aimo Kannt, C. Roy D. Lancaster, and Hartmut Michel
Abteilung Molekulare Membranbiologie, Max-Planck-Institut für Biophysik, D-60528 Frankfurt am Main, Germany

ABSTRACT We have calculated the electrostatic potential and interaction energies of ionizable groups and analyzed the response of the protein environment to redox changes in *Paracoccus denitrificans* cytochrome *c* oxidase by using a continuum dielectric model and finite difference technique. Subsequent Monte Carlo sampling of protonation states enabled us to calculate the titration curves of all protonatable groups in the enzyme complex. Inclusion of a model membrane allowed us to restrict the calculations to the functionally essential subunits I and II. Some residues were calculated to have complex titration curves, as a result of strong electrostatic coupling, desolvation, and dipolar interactions. Around the heme a_3-Cu_B binuclear center, we have identified a cluster of 18 strongly interacting residues that account for most of the proton uptake linked to electron transfer. This was calculated to be between 0.7 and 1.1 H^+ per electron, depending on the redox transition considered. A hydroxide ion bound to Cu_B was determined to become protonated to form water upon transfer of the first electron to the binuclear site. The bulk of the protonation changes linked to further reduction of the heme a_3-Cu_B center was calculated to be due to proton uptake by the interacting cluster and $Glu^{II\text{-}78}$. Upon formation of the three-electron reduced state (P1), His^{325}, modeled in an alternative orientation away from Cu_B, was determined to become protonated. The agreement of these results with experiment and their relevance in the light of possible mechanisms of redox-coupled proton transfer are discussed.

GLOSSARY

$\Delta G_{crg}(i, j)$	charge-charge interaction energy between fully ionized residues i and j
ΔG_{rxn}	reaction field energy
$\Delta\Delta G_{rxn}$	"desolvation penalty," difference in ΔG_{rxn} for residue i in solution and in the protein
ΔG_{pol}	interaction energy of residue i with permanent dipoles
ΔpK_{desolv}	change in pK arising from the "desolvation penalty"
ΔpK_{pol}	change in pK arising from ΔG_{pol}
pK_{int}	"intrinsic pK," pK of an ionizable residue i if all other groups were neutral
Pra/Prd *a*	ring A/D heme propionates of heme *a*
Pra/Prd a_3	ring A/D heme propionates of heme a_3

Energy units

1 ΔpK unit = 1.38 kcal/mol = 5.77 kJ/mol = 0.06 eV

INTRODUCTION

Cytochrome *c* oxidase is the terminal complex of the respiratory chains of aerobic organisms. It is located in the inner membrane of mitochondria and many bacteria, and catalyzes electron transfer from cytochrome *c* to molecular oxygen, reducing the latter to water. The reaction is accompanied by vectorial proton transport through the membrane, a process that is generally referred to as proton pumping. The resulting proton and voltage gradient is then employed by the F_0F_1-ATP synthase for phosphorylation of ADP, yielding ATP. The structure of the oxidized, azide-treated cytochrome *c* oxidase from the soil bacterium *Paracoccus denitrificans* has been determined by x-ray crystallography at 2.8-Å resolution (Iwata et al., 1995). The protein consists of four subunits (cf. Fig. 3 *a*); subunit I is the largest, with 12 transmembrane helices arranged in three symmetry-related semicircles. Subunit II contains two transmembrane helices and a large periplasmic domain with a fold similar to that of type I copper proteins. Subunits III and IV consist of seven and one transmembrane helices, respectively, and only small periplasmic or cytoplasmic segments. The three mitochondrially encoded subunits of the 13-subunit bovine heart enzyme, the crystal structure of which was reported recently at 2.8 Å (Tsukihara et al., 1996), were found to be remarkably similar to their bacterial homologs.

Cytochrome *c* oxidase contains four redox-active cofactors: a Cu_A, a low-spin heme (heme *a*) and a heme a_3-Cu_B binuclear center. The hemes and Cu_B are located in subunit I, and the Cu_A center belongs to subunit II. Electrons from cytochrome *c* are accepted by Cu_A and then transferred via heme *a* to the binuclear center, where oxygen reduction takes place. The catalytic cycle of the oxygen reduction is summarized in Fig. 1 (Babcock and Wikström, 1992, with modifications). Upon uptake of the first electron by the fully oxidized (O) enzyme, the one-electron reduced intermediate (E) is formed, which subsequently becomes further reduced to the two-electron reduced R-state to which oxygen can bind. Oxygen binding, via formation of compound A

Received for publication 30 July 1997 and in final form 4 November 1997.

Address reprint requests to Dr. Hartmut Michel, Abteilung Molekulare Membranbiologie, Max-Planck-Institut für Biophysik, Heinrich-Hoffmann-Strasse 7, D-60528 Frankfurt am Main, Germany. Tel.: 49-69-96769-401; Fax: 49-69-96769-423; E-mail: michel@mpibp-frankfurt.mpg.de.

Amino acid numbering refers to the *Paracoccus denitrificans* cytochrome *c* oxidase. If not otherwise indicated by roman numerals between residue type and sequence number, residues belong to subunit I.

0006-3495/98/02/708/14 $2.00

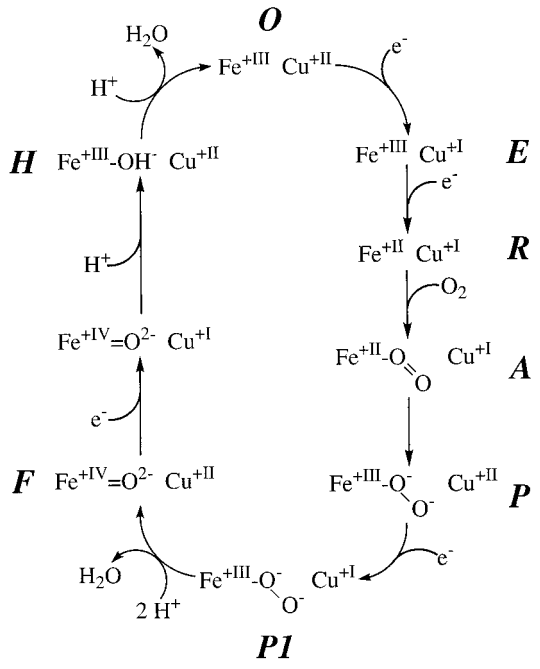

FIGURE 1 Short version of the catalytic cycle of cytochrome *c* oxidase (Babcock and Wikström, 1992, with modifications). Fe and Cu represent heme a_3 and Cu_B, respectively. Bold italic letters refer to different redox states of the binuclear site, namely the fully oxidized state (***O***), the one-electron reduced intermediate (***E***), the fully reduced state (***R***) that is converted into compound A upon oxygen binding, the peroxy state before (***P***) and after (***P1***) uptake of the third electron, the oxoferryl (***F***) state, and the hydroxy state (***H***).

(Chance et al., 1975), leads to the peroxy state P, the structure of which is still uncertain. Transfer of the third electron via Cu_A and heme *a* then traps the oxygen within the binuclear center (Verkhovsky et al., 1994, 1996); the corresponding intermediate is referred to as P1. Upon scission of the O-O bond and formation of the first water molecule, the stable oxoferryl or F-state is produced (Varotsis and Babcock, 1990). Input of the fourth electron leads to the hydroxy intermediate H and, after release of the second water molecule, to the regeneration of the O-state.

The associated generation of a proton gradient across the membrane is the outcome of two processes: the uptake of "chemical" protons from the cytoplasm that are required for water formation and the translocation of "pumped" protons from the cytoplasm into the periplasm. Analysis of membrane potential effects (Wikström, 1989) and time-resolved charge-translocation measurements on reconstituted enzyme (Verkhovsky et al., 1997) have shown that only the P $\rightarrow$ F and F $\rightarrow$ O transitions are coupled to proton pumping. However, the molecular mechanism by which this coupling is achieved is still unclear. Previous proposals involve ligand exchanges and protonations on Cu_B (Wikström et al., 1994), on heme a_3 (Rousseau et al., 1993), or between the two metals (Woodruff, 1993). On the grounds of possible multiple orientations and conformations for the side chain of the Cu_B ligand His^{325}, Iwata et al. (1995) have favorably discussed the "histidine cycle" model of Wikström et al. (1994), with the histidine cycling through two different orientations and three different protonation states dependent on the redox state of the enzyme. The model is in agreement with the electroneutrality principle (Rich, 1995), which postulates that reduction of the binuclear center causes the uptake of protons from the cytoplasm to maintain electroneutrality. These protons are then expelled into the periplasm through electrostatic repulsion from the incoming "chemical" protons required for water formation. Critical within such a model is the identity of the groups that become protonated upon electron transfer to the binuclear site.

Two different pathways for chemical and pumped protons were indicated by site-directed mutagenesis experiments where the mutation prevented proton pumping but still allowed water formation (Thomas et al., 1993; Fetter et al., 1995; Garcia-Horsman et al., 1995). Iwata et al. (1995) proposed two such pathways for the *Paracoccus* enzyme. The pathway for protons to be consumed involves residues Ser^{291}, Lys^{354}, Thr^{351}, and Tyr^{280}, and the pathway for protons to be pumped was suggested to include Asp^{124}, Thr^{203}, Asp^{199}, Asp^{113}, Asp^{131}, and Tyr^{35}. Beyond the latter residue, a presumably solvent-filled cavity leads to the highly conserved Glu^{278}. From there the pathway seems less clear but may involve Pro^{277}, from which it could reach the binuclear site.

However, recent investigations using site-directed mutants (Konstantinov et al., 1997) indicate that the former pathway may be used in the first, so-called eu-oxidase part of the catalytic cycle, whereas the latter pathway is of importance only for the second, peroxidase part of the reaction.

The aim of the work presented here was to gain further insight into the coupling of proton translocation to electron transfer by using electrostatic calculations. Similar methods have recently been applied to other systems such as the photosynthetic reaction centers of *Rb. sphaeroides* (Beroza et al., 1995; Gunner and Honig, 1992) and *Rp. viridis* (Lancaster et al., 1996). A continuum dielectric model and finite difference technique were used to determine the electrostatic potential in and around cytochrome *c* oxidase and to identify residues that are strongly electrostatically coupled. Monte Carlo sampling allowed the determination of the average protonation of all titratable residues as a function of pH and dependent on the redox state of the enzyme.

METHODS

Coordinates

Calculations were based on the nonhydrogen coordinates of subunits I and II of the *P. denitrificans* enzyme (Protein Data Bank (PDB) entry code 1ar1, Ostermeier et al., 1997). This set of coordinates contains a magnesium ion bound to His^{403}, Asp^{404}, $Glu^{II\text{-}218}$ and a water molecule, similar to the Mg site proposed for the bovine heart enzyme (Tsukihara et al., 1995).

Fann et al. (1995), through extended x-ray absorption fine structure and electron nuclear double-resonance spectroscopy experiments at high pH,

have suggested a water molecule or hydroxide ion as a fourth ligand to Cu_B that could account for the strong antiferromagnetic coupling of the heme a_3 iron and the copper. This water was modeled (Fig. 2 *a*) at a distance of 1.95 Å from the copper, in agreement with the data of Fann et al. (1995), assuming a distorted tetrahedral coordination of the copper center. It was generally included, but was omitted from a separate series of calculations, as indicated in the Results section. For the relevant redox states, an oxygen molecule bound to heme a_3 was modeled in analogy to the heme-bound oxygen molecule in oxygenated hemoglobin (Condon and Royer, 1994).

Because, in the original structure obtained with the oxidized enzyme in the presence of azide (Iwata et al., 1995), the orientation of the Cu_B ligand His^{325} could not be observed crystallographically, its side chain was modeled in two different conformations: as a ligand to Cu_B and in an alternative orientation away from the copper (cf. Fig. 2 *b*; see Results section for details).

We have included a membrane model (Fig. 3 *b*) that shields the membrane-exposed protein surface from the solvent. The membrane is represented by a lattice of carbon atoms that are 3 Å apart and form a layer of thickness 27 Å, mimicking the hydrophobic part of the membrane (Lancaster et al., manuscript in preparation). Inclusion of this membrane model also allowed us to restrict the calculations to subunits I and II, saving CPU time. Previous studies have shown that the two-subunit enzyme is active in proton pumping (Haltia et al., 1989; Hendler et al., 1991).

Protons were added with the program PROTEUS (A. Joguine and M. R. Gunner, City College of New York, unpublished observations), which is distributed as part of the GRASP package (Nicholls et al., 1991). This program orients protons on water molecules or hydroxyl groups to minimize the electrostatic interaction free energy of the proton with residues within 4.5 Å of the considered group.

Calculation of electrostatic energies and individual site titration curves

Calculations were performed as developed by M. R. Gunner (City College New York), implemented locally by Lancaster (1996), and described by Lancaster et al. (1996). The program DelPhi (Gilson et al., 1987; Nicholls and Honig, 1991) was used to solve the Poisson equation for the electrostatic potential in and around cytochrome *c* oxidase. The protein interior was assigned a dielectric constant of 4, whereas 80 was used for the solvent. The molecular surface of the protein as the boundary between high- and low-dielectric media was defined by a solvent probe of radius 1.4 Å (Connolly, 1983). A series of four focusing calculations was performed with a final grid spacing of 1.0 Å/grid.

Charge distributions for amino acid side chains were taken from the CHARMM set of charges (Brooks et al., 1983). Arg, Asp, Cys, Glu, His, Lys, and Tyr residues, heme propionates, and chain termini were treated as titratable residues. However, histidines liganding copper atoms or heme irons were considered neutral. Preliminary calculations explicitly including the possibility of deprotonation of the Cu_B-ligating histidines to their imidazolate forms showed the histidines to be already neutral in the fully oxidized state of the enzyme. Furthermore, treating the His ligands as deprotonatable is problematic, because of the present level of resolution, the absence of model compounds, and the resulting uncertainty about the correct metal-to-ligand distances, to which the ionization states of the ligands are highly sensitive. The copper atoms were given charges of 0.75/0.25 and 1.0/0.0 for the oxidized/reduced forms of Cu_A and Cu_B, respectively. The remaining charges of 0.75 and 1.0 for Cu_A and Cu_B were evenly distributed over the liganding atoms. Thus, in the case of Cu_B, the ligating histidines were given a +0.33 charge on their ligating atoms or, when a hydroxide ion was included as a fourth ligand, a +0.25 charge, and the remaining +0.25 was assigned to the hydroxide, giving it a net charge of −0.75. Charge assignments to the heme atoms were as described by Lancaster et al. (1996); additional partial charges were put on the formyl (+0.55/−0.55 for the carbon and oxygen atoms, respectively) and hydroxyalkyl groups (C: +0.25, O: −0.65, H: +0.40).

The electrostatic contribution to the free energy of a charge in the protein is the sum of three different energy terms: the reaction field energy, ΔG_{rxn}, the dipolar interaction energy, ΔG_{pol}, and the interaction energy with other ionizable residues, ΔG_{crg}.

The reaction field energy accounts for the polarization of electrons and dipoles in the surrounding medium, which stabilizes a charge. Transferring a charge from such a high-dielectric medium into an environment with a low dielectric constant leads to a loss of reaction field energy, $\Delta\Delta G_{rxn}$, which is often referred to as the desolvation penalty. Thus, in a low-dielectric medium, the protonation equilibrium of a titratable residue is shifted toward the neutral form, resulting in a change in pK, ΔpK_{desolv}.

The term ΔG_{pol} takes into account the interaction with permanent dipoles such as the polar groups of the protein backbone or polar amino acid side chains. pK changes due to $\Delta\Delta G_{rxn}$ and ΔG_{pol} can be combined to yield the "intrinsic" pK, pK_{int}, which is the pK of the considered group when all other titratable residues in the protein are in their neutral state

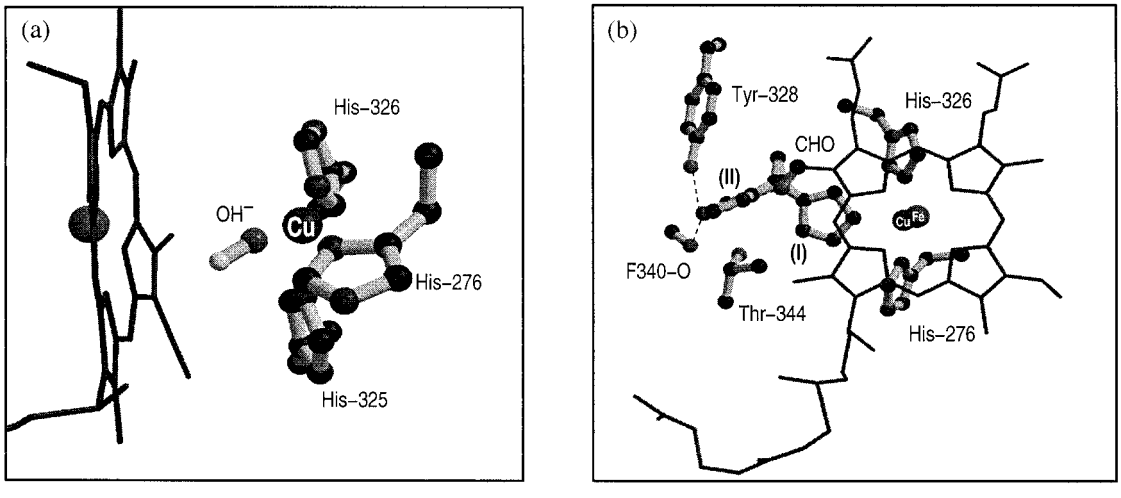

FIGURE 2 (*a*) The binuclear center with a hydroxide ion bound to Cu_B. (*b*) His^{325} was modeled in two different orientations as indicated by Iwata et al. (1995): as a ligand to Cu_B (I) and in its "free" orientation (II) hydrogen-bonded to the heme a_3 formyl group (CHO), the carbonyl oxygen of Phe^{340}, and the OH group of Tyr^{328}. Hydrogen bonds are depicted as dashed lines. Both images were prepared with MolScript (Kraulis, 1991) and Raster3D (Bacon and Anderson, 1988; Merrit and Murphy, 1994).

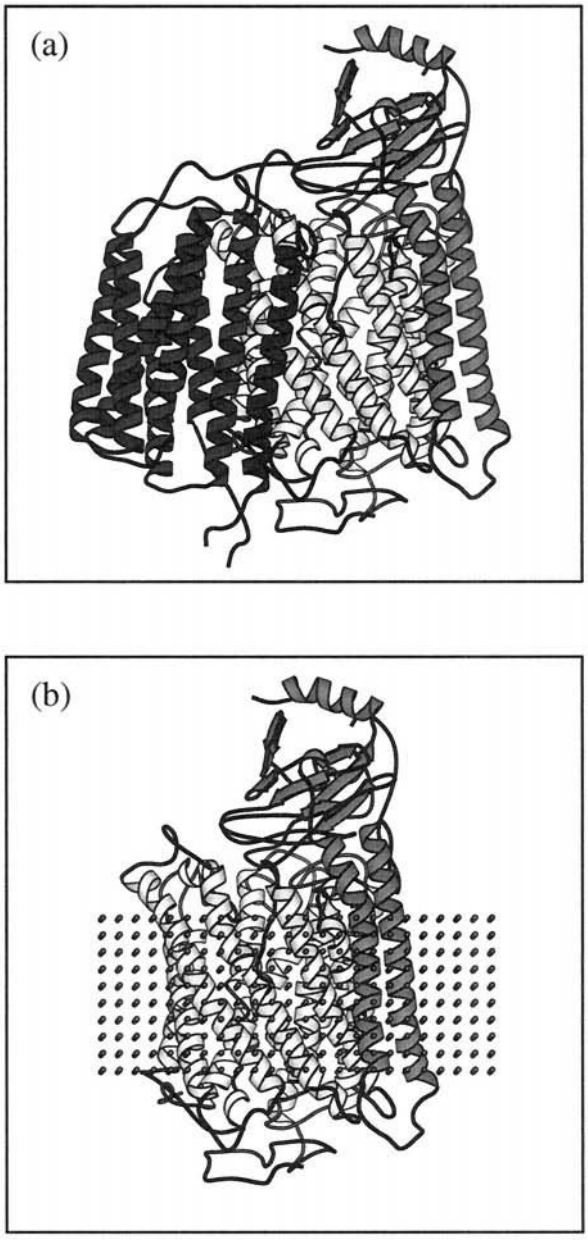

FIGURE 3 (*a*) Structure of the four-subunit cytochrome *c* oxidase from *Paracoccus denitrificans* (Iwata et al., 1995). Subunits I, II, III, and IV are shown in white, light grey, dark grey, and black, respectively. (*b*) Subunits I and II with the membrane model. The hydrophobic part of the membrane is represented by a matrix of carbon atoms (shown as *grey balls*) surrounding the protein. Both images were prepared with MolScript.

(Tanford and Kirkwood, 1957):

$$pK_{int} = pK_{sol} - c_a(\Delta pK_{desolv} + \Delta pK_{pol})$$

where pK_{sol} is the pK_a of the titrating group in solution and c_a is -1 for an acidic and $+1$ for a basic group, respectively. It should be noted that in the above equation ΔpK_{desolv} is always nonnegative, whereas ΔpK_{pol} is positive for basic and negative for acidic residues when $\Delta G_{pol} > 0$, and vice versa when $\Delta G_{pol} < 0$.

Unlike $\Delta\Delta G_{rxn}$ and ΔG_{pol}, ΔG_{crg} is dependent on pH in that it is a function of the average protonation $\langle x_i \rangle$ for all titratable residues i within the protein. It is possible to compute $\langle x_i \rangle$ by calculating the complete partition function. However, for proteins with more than 25 titration sites, this approach becomes prohibitively time-consuming. Instead, we have used a Monte Carlo algorithm as described by Lancaster et al. (1996) to calculate individual site titration curves for different redox states of the enzyme. A total of 3.2×10^6 Monte Carlo steps (after 1.6×10^6 pre-equilibration steps) were applied to determine the average ionization of each site over the pH region between 4.0 and 11.5. Strongly coupled residues with a $\Delta\Delta G_{crg}$ greater than 2 ΔpK units were permitted to change their protonation state simultaneously in a single Monte Carlo step over 50% of the time, as suggested by Beroza et al. (1991).

Water molecules, with the exception of the ligands to the magnesium and the binuclear site, were not explicitly included in the calculations. It has been pointed out by Yang et al. (1993) and Lancaster et al. (1996) that the explicit treatment of buried water molecules is difficult, because there are no unique positions for the water hydrogen atoms. Upon protonation or deprotonation of a nearby residue, the hydrogen atoms might change their position to stabilize the protonation state of the residue through the formation of hydrogen bonds. As our approach cannot account for such positional fluctuations, the error introduced by explicitly including the buried waters may well be greater than the error caused by leaving them out. However, our version of DelPhi implicitly includes the stabilization of charges or dipoles by assigning a dielectric constant of 80 to each cavity within the protein that is large enough to accommodate a water molecule. Hence bound water molecules are treated as a high-dielectric continuum, which, however, underestimates the stabilization effects of highly directed hydrogen bonds (Yang et al., 1993). As shown by Yang et al. (1993) in a study with T4 lysozyme, the likely deviation from experimental values introduced by the continuum approximation can extend to ~2 ΔpK units. In their case, explicitly including bound waters was found to only marginally improve the agreement with experiment.

RESULTS

Electrostatic interactions between residues in the fully oxidized state

Subunits I and II of cytochrome *c* oxidase contain 151 residues that were considered protonatable: 19 Arg, 26 Asp, 6 nonligated Cys, 25 Glu, 15 nonligated His, 18 Lys, 36 Tyr, 4 heme propionates, 1 C-terminus and 1 N-terminus (residues 1–16 and 550–554 of subunit I are not defined in the crystal structure). In addition, two water molecules were explicitly included, as described in the Methods section. A "core" cluster of 18 of these 151 titratable residues (cf. Table 1) was found to strongly electrostatically interact with the cofactors, either directly or indirectly (i.e., via other titratable residues). The term "strong" is used for interactions that correspond to a change in pK by at least 2 ΔpK units, that is, with interaction energies larger than 2.74 kcal/mol. Tyr (with the exception of Tyr^{280}; see below) and Cys residues were omitted from the cluster because they were calculated to be neutral in all redox states and at all pH values.

Calculated desolvation penalties and polar interaction energies are included in Table 1. The loss of reaction field energy, $\Delta\Delta G_{rxn}$, can become large enough to shift the pK_a by as much as 12.9 ΔpK units. The latter value applies to the ring A propionate of heme *a* (Pra *a*), the carboxyl oxygens of which are ~10 Å away from the protein-solvent boundary.

The term in addition to $\Delta\Delta G_{rxn}$ that influences the intrinsic pK is the charge-dipole interaction energy, ΔG_{pol}. It arises from interactions with polar side chains and dipoles

TABLE 1 The core cluster of strongly electrostatically interacting residues

a)		Asp	CuA	Asp	Asp	Glu	Mg	Pra	Asp	Lys	Arg	Arg	His	Heme	Pra	Prd	Arg	Arg	Prd	Heme	Glu	Wat	CuB	Tyr
		II		I	II	II		a_3	I	II	I	I	I	a	a	a	I	I	a_3	a_3	I			I
		178		404	193	218			399	191	400	54	464				473	474			278			280
	Asp-II-178		3.1	0.5	0.7	0.4	-0.7	0.4	0.3	-0.4	-0.3	-0.2	-0.2	-0.3	0.4	0.5	-0.5	-0.7	0.5	-0.3	0.2	0.2	-0.3	0.2
	CuA	3.1		-3.4	-3.6	-0.8	4.0	-2.2	-1.7	2.7	1.1	1.2	0.9	1.3	-2.8	-2.6	2.7	3.5	-2.4	1.1	-0.8	-0.9	1.1	-0.7
	Asp-I-404	0.5	-3.4		3.7	3.6	-11.7	4.0	2.7	-3.1	-1.1	-1.0	-1.0	-1.4	2.5	3.0	-4.4	-4.6	3.9	-1.6	0.9	1.3	-1.7	0.9
	Asp-II-193	0.7	-3.6	3.7		3.8	-8.0	3.6	2.9	-3.0	-2.0	-0.7	-0.8	-1.1	1.6	2.3	-3.2	-3.6	3.5	-1.5	0.9	1.3	-1.7	1.0
	Glu-II-218	0.4	-0.8	3.6	3.8		-9.0	2.7	1.7	-1.2	-0.7	-0.5	-0.6	-0.8	1.1	2.0	-2.8	-3.5	3.3	-1.2	0.8	1.0	-1.4	0.7
	Mg	-0.7	4.0	-11.7	-8.0	-9.0		-5.5	-4.0	4.1	1.8	1.1	1.2	1.6	-2.4	-3.4	5.0	5.4	-5.1	2.1	-1.2	-1.8	2.4	-1.3
	Pra a_3	0.4	-2.2	4.0	3.6	2.7	-5.5		11.7	-3.5	-2.0	-1.3	-2.2	-2.0	2.4	3.1	-5.5	-4.2	5.9	-4.6	1.5	3.6	-4.3	2.3
	Asp-I-399	0.3	-1.7	2.7	2.9	1.7	-4.0	11.7		-4.1	-3.5	-1.0	-2.0	-1.4	1.7	1.9	-3.0	-2.5	3.3	-3.4	1.1	2.6	-3.2	2.0
	Lys-II-191	-0.4	2.7	-3.1	-3.0	-1.2	4.1	-3.5	-4.1		2.5	1.1	1.5	1.1	-1.7	-1.6	2.3	1.9	-2.0	1.4	-0.6	-1.1	1.3	-0.9
	Arg-I-400	-0.3	1.1	-1.1	-2.0	-0.7	1.8	-2.0	-3.5	2.5		0.4	0.7	0.5	-0.7	-0.8	1.1	1.1	-1.1	1.1	-0.4	-0.9	1.1	-0.8
	Arg-I-54	-0.2	1.2	-1.0	-0.7	-0.5	1.1	-1.3	-1.0	1.1	0.4		2.3	4.1	-4.7	-2.2	2.3	1.5	-1.5	1.2	-0.8	-0.8	0.9	-0.8
	His-I-464	-0.2	0.9	-1.0	-0.8	-0.6	1.2	-2.2	-2.0	1.5	0.7	2.3		2.3	-1.8	-1.5	1.9	1.2	-1.8	2.8	-0.9	-1.6	1.7	-1.6
	Heme a	-0.3	1.3	-1.4	-1.1	-0.8	1.6	-2.0	-1.4	1.1	0.5	4.1	2.3		-4.8	-4.9	4.1	2.6	-3.3	2.5	-2.2	-1.6	1.9	-1.6
	Pra a	0.4	-2.8	2.5	1.6	1.1	-2.4	2.4	1.7	-1.7	-0.7	-4.7	-1.8	-4.8		7.3	-6.7	-4.5	3.3	-1.7	1.2	1.2	-1.4	1.0
	Prd a	0.5	-2.6	3.0	2.3	2.0	-3.4	3.1	1.9	-1.6	-0.8	-2.2	-1.5	-4.9	7.3		-10.3	-13.6	6.2	-2.3	2.1	1.8	-2.2	1.4
	Arg-I-473	-0.5	2.7	-4.4	-3.2	-2.8	5.0	-5.5	-3.0	2.3	1.1	2.3	1.9	4.1	-6.7	-10.3		7.6	-11.0	3.1	-1.9	-2.4	2.9	-1.7
	Arg-I-474	-0.7	3.5	-4.6	-3.6	-3.5	5.4	-4.2	-2.5	1.9	1.1	1.5	1.2	2.6	-4.5	-13.6	7.6		-6.5	2.2	-1.8	-1.9	2.4	-1.4
	Prd a_3	0.5	-2.4	3.9	3.5	3.3	-5.1	5.9	3.3	-2.0	-1.1	-1.5	-1.8	-3.3	3.3	6.2	-11.0	-6.5		-4.3	2.6	3.7	-4.5	2.4
	Heme a_3	-0.3	1.1	-1.6	-1.5	-1.2	2.1	-4.6	-3.4	1.4	1.1	1.2	2.8	2.5	-1.7	-2.3	3.1	2.2	-4.3		-2.6	-12.9	9.6	-8.4
	Glu-I-278	0.2	-0.8	0.9	0.9	0.8	-1.2	1.5	1.1	-0.6	-0.4	-0.8	-0.9	-2.2	1.2	2.1	-1.9	-1.8	2.6	-2.6		2.3	-3.1	2.7
	Wat	0.2	-0.9	1.3	1.3	1.0	-1.8	3.6	2.6	-1.1	-0.9	-0.8	-1.6	-1.6	1.2	1.8	-2.4	-1.9	3.7	-12.9	2.3		-20.9	6.5
	CuB	-0.3	1.1	-1.7	-1.7	-1.4	2.4	-4.3	-3.2	1.3	1.1	0.9	1.7	1.9	-1.4	-2.2	2.9	2.4	-4.5	9.6	-3.1	-20.9		-8.2
	Tyr-I-280	0.2	-0.7	0.9	1.0	0.7	-1.3	2.3	2.0	-0.9	-0.8	-0.8	-1.6	-1.6	1.0	1.4	-1.7	-1.4	2.4	-8.4	2.7	6.5	-8.2	
b)																								
	ΔpK_{desolv}	4.5		9.5	7.7	9.1		12.0	10.2	8.3	6.3	8.8	11.6		12.9	12.6	7.4	5.6	10.5		8.3	12.6		15.5
	ΔpK_{pol}	-7.3		-3.2	-2.3	-3.3		-5.6	-2.9	-5.6	-4.4	-6.0	-3.5		-12.0	-10.6	6.4	6.0	-4.4		1.7	5.7		2.7
	pK_{int}	1.1			9.3			10.2	11.2	8.2	10.5	9.7	-1.6		4.8	5.9	-1.2	0.9	9.9		14.3	33.4		29.1

a. pH-dependent charge-charge interaction energies (ΔG_{crg}) in ΔpK units for residues that strongly electrostatically interact with the cofactors. Values greater than 2 ΔpK units are highlighted in bold; values greater than 5 ΔpK units are shown white-on-black. Charge-charge interaction energies with the charged but nontitratable metal atoms of Cu_A, Cu_B, Mg, and the Fe atoms of hemes *a* and a_3 are also included. For clarity, the information in the symmetrical matrix is duplicated on both sites of the diagonal.

b. pK shifts arising from the loss of reaction field energy (ΔpK_{desolv}) and pH-independent polar interactions (ΔpK_{pol}) that contribute to the intrinsic pK (pK_{int}) of the amino acid residues of *Paracoccus denitrificans* cytochrome *c* oxidase. Solution pK (pK_{sol}) values: 12.5 (Arg), 3.9 (Asp), 4.3 (Glu), 6.5 (His), 10.8 (Lys), 3.8 (Pra/Prd), 15.7 (Wat).

of the protein backbone and can often compensate for the loss of reaction field energy. The latter, for example, is the case for the two heme *a* propionates, where the charged state is stabilized by 12.0 (ring A propionate, Pra) and 10.6 (ring D propionate, Prd) ΔpK units, respectively. For Pra, this is mainly due to interactions with the backbone carbonyls of Arg^{473} and Arg^{474}, the formyl group of heme *a*, and the amide group of the Trp^{475} indole ring. In the case of Prd, charge stabilization is the result of interactions with the backbone carbonyl groups of residues 88, 94, 95, 163, and 164, and the side-chain amide group of Asn^{88}.

However, the region of positive potential around the heme *a* propionates (cf. Fig. 4 for the contribution of the backbone to ΔG_{pol}) has the opposite effect on the two arginines 473 and 474, i.e., the charged state of these two residues is further destabilized through polar interactions. For Arg^{474}, this mainly results from interactions with the backbone carbonyl groups of residues 163–166 and 170 that are oriented with the carbonyl oxygen atoms pointing away from the protonatable groups of the arginine.

A region of negative potential generated by polar sites was found around Arg^{54}, stabilizing the protonated state of the arginine. This occurs despite a strong interaction with the side-chain amide of Asn^{486}, which destabilizes the charge by 3.7 ΔpK units, as that is overcompensated by interactions with the side chains of Gln^{463}, Ser^{489}, Ser^{490} and the heme *a* formyl group (together −7.3 ΔpK units) and the backbone carbonyl groups of residues 50, 459, 482, 483, 486, 487, and 490 (−3.3 ΔpK units; cf. Fig. 4).

Within the core of interacting titratable residues mentioned above, there are 69 charge-charge interactions with energies greater than 2 ΔpK units, not including the interactions with the cofactor metals. One of the strongest interactions is that between Asp^{399} and the ring A propionate of heme a_3 (Pra a_3). The two carboxyl groups are only 3.3 Å apart at their closest oxygen-oxygen distance (cf. Fig. 6). The deprotonated state of one of the two residues is thus destabilized by the charged state of the other, whereas the net protonation of the coupled system Asp^{399} + Pra a_3 will depend on the interaction with the environment. Consequently, the two groups were found to share a single proton over the whole pH range considered. Other very strong charge-charge interaction energies (>10 ΔpK units), although between oppositely charged groups, were determined for the interaction of the two arginines 473 and 474 with the ring D propionates of hemes *a* and a_3.

The charge-charge interaction energy between the two hemes was calculated as 2.5 ΔpK units. Thus, reduction of either heme will lower the midpoint potential and hence decrease the affinity for electrons of the other heme by ~145 mV (as proposed in the "neoclassical model" by Nicholls, 1974), a value that is in reasonable agreement with

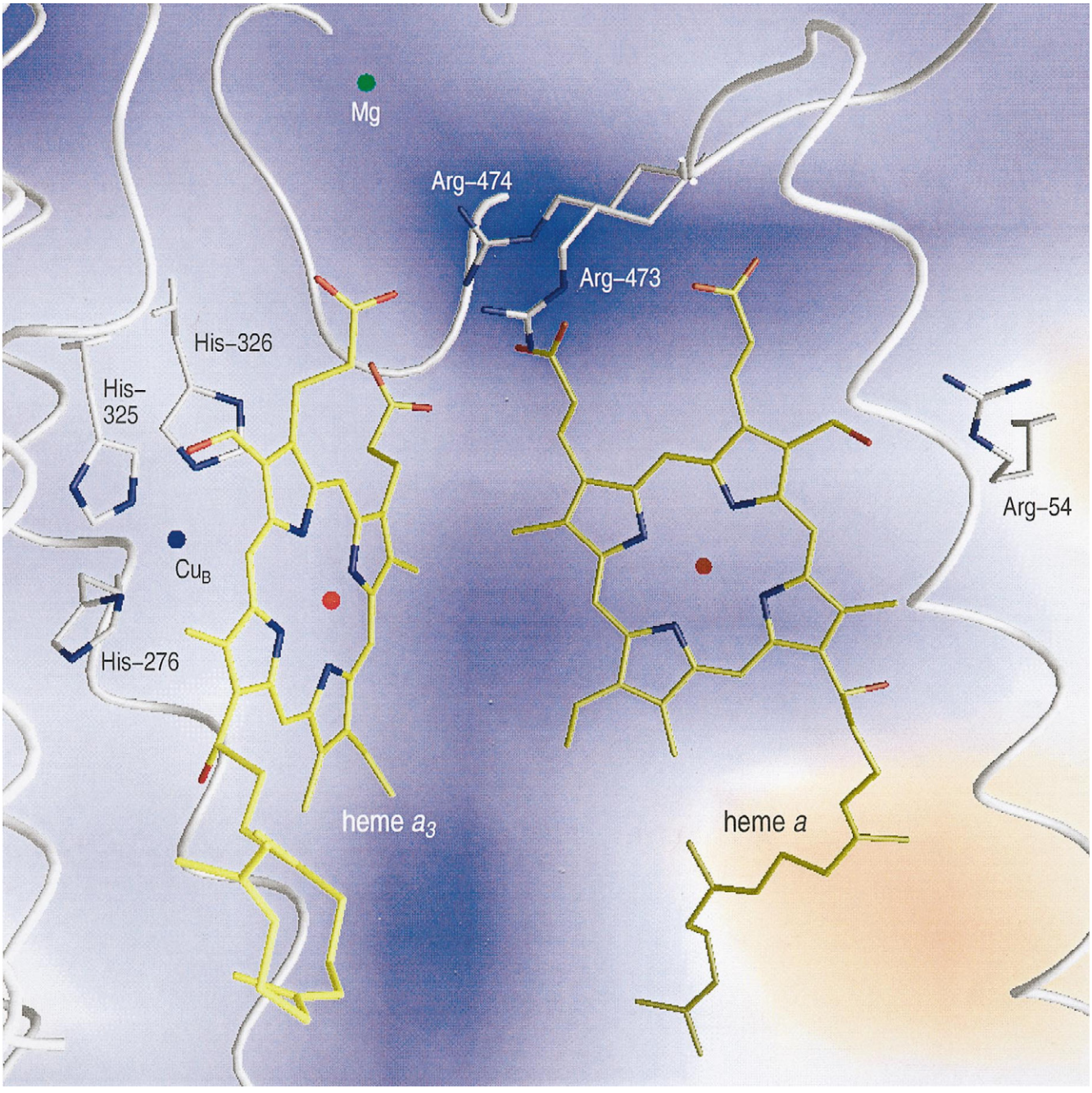

FIGURE 4 Contribution of the polypeptide backbone to the electrostatic potential in cytochrome *c* oxidase. Depicted is a slice plane running through the NH2 atom of Arg^{474}. Zones of negative and positive potential are coloured red and blue, respectively, with the most intense colors corresponding to −300 and +750 mV. Values for residues shown are −260, 390, and 420 mV, respectively, for Arg^{54}, Arg^{473}, and Arg^{474} (average of NH1 and NH2 atoms). The heme irons, Cu_B, and Mg are shown as red, blue, and green balls, respectively. The figure was prepared with GRASP (Nicholls et al., 1991).

the experimentally determined value of 124 mV (Wilson et al., 1972; reviewed by Wikström et al., 1976).

Calculation of titration curves

Individual site titration curves were calculated for different redox states of the enzyme by Monte Carlo sampling. The isoelectric point for the fully oxidized state of the enzyme was determined as 4.6, a value that agrees well with the experimentally observed value (4.5; C. Ostermeier, personal communication). At pH 7.0, all Arg, all but seven Asp, all but nine Glu, all but four Lys, and the four heme propionates were determined to be fully charged, whereas all but three His, and all nonligated Cys and Tyr (with the exception of Tyr^{280}; see below) residues were found to be in their neutral states.

Titration patterns of many residues deviate significantly from the standard Henderson-Hasselbalch curve for a single

titratable site, as previously reported for other systems (Bashford and Gerwert, 1992; Beroza et al., 1995; Lancaster et al., 1996). Some residues have fixed protonation states over the whole pH range (4–11.5) of the calculations. For example, Lys^{354} was determined to be in its neutral state over the entire pH range considered, which is due to the large desolvation penalty of 11.1 ΔpK units and the lack of significant compensating dipolar or charge-charge interactions. Control calculations using the coordinates of the bovine heart enzyme (POB entry code, 10CC, Tsukihara et al., 1996) yielded the same result (data not shown).

For other residues, however, large desolvation penalties and unfavorable polar interactions were found to be overcompensated by charge-charge interactions that stabilize the charged state. Arg^{473}, for instance, was calculated to be fully protonated (i.e., charged) between pH 4 and 11.5, despite having an intrinsic pK of as small as −1.2. This is due to strong electrostatic interactions with 17 other residues and cofactors, the strongest ones being with two heme propionates and Arg^{474}. The salt bridges to the ring D propionates of hemes *a* and a_3 alone stabilize the charged state of Arg^{473} by 21.3 ΔpK units (Table 1) and are only partially compensated for by the charge-destabilizing interaction with Arg^{474} (7.6 ΔpK units). Another example is the residue $Asp^{II\text{-}35}$, which, though having a pK_{int} of 7.9, was calculated to be fully deprotonated. The main reason for this is a salt bridge to Arg^{468} (su I) that alone shifts the pK_a of the aspartate by as much as −7.5 ΔpK units. Correspondingly, the arginine was calculated to be fully protonated between pH 4 and 11.5. This salt bridge could contribute significantly to the stabilization of the multisubunit complex.

As already mentioned, Asp^{399} and Pra a_3 were calculated to share a single proton between pH 4 and 11.5. As a result of an additional hydrogen bond to the propionate from His^{403}, Pra a_3 was determined to be fully charged (i.e., the proton was calculated to reside on Asp^{399}).

Dependence of the average protonation on the redox state

Upon reduction of a cofactor, the protonation equilibria of nearby titratable residues are altered as the loss of a positive charge destabilizes the charged state of acidic and stabilizes the protonated state of basic residues. In this study we have modeled the catalytic cycle of cytochrome *c* oxidase (see Fig. 1) and calculated the electrostatic response and changes in protonation linked to changes in the redox state of the protein. We will focus mainly on the protonation changes that occur in response to electron transfer to the heme a_3–Cu_B binuclear center.

Changes in average protonation upon reduction of the binuclear center

Starting at the fully oxidized state of the enzyme, the first electron is accepted by Cu_A and then transferred via heme *a* to the binuclear site, forming the so-called one-electron reduced intermediate E (Babcock and Wikström, 1992). Uptake of the second electron and subsequent transfer to the binuclear center lead to the R state in which the binuclear center is fully reduced and ready to bind an oxygen molecule (Fig. 1).

Calculated changes in average protonation linked to redox reactions at the binuclear site are summarized in Table 2 and Fig. 5. Upon formation of the E-intermediate, the net protonation of the enzyme was found to increase by 1.0 H^+ as compared to the O state (pH 7). Apart from the hydroxide ion bound to the binuclear site, which was calculated to become fully protonated, no other residues contribute significantly to the overall change in protonation. The hydroxide becoming protonated to water could be important for the function of the enzyme in that it would raise the redox potential of heme a_3, thereby speeding up the heme-heme electron transfer. Verkhovsky et al. (1995) have found that this electron transfer reaction is controlled by proton uptake and proposed a protonatable site very close to the binuclear center whose protonation triggers the electron transfer. The hydroxide ligand appears to be a likely candidate. Furthermore, its protonation would allow the newly formed water molecule to dissociate from the reduced binuclear site, thus allowing oxygen to bind.

Further reduction of the binuclear center (i.e., formation of the R state) was calculated to be associated with an increase in the average protonation of $Lys^{II\text{-}191}$ and $Glu^{II\text{-}78}$ by 0.58 and 0.23 H^+, respectively, which mainly contribute to an overall proton uptake of 0.8 H^+ (compared to the E state).

Before uptake of the third electron, oxygen reversibly binds to the binuclear site, forming the so-called compound

TABLE 2 Average protonation of selected residues for different redox states of the binuclear center

Redox state*	$e^{\#}$	$H^{+\,\S}$	$Lys^{II\text{-}191}$	$Glu^{II\text{-}78}$	$OH^{-\,\P}$	$His^{325\,\|\|}$	Tyr^{280}
O	0	—	0.10	0.30	0.00		1.00
E	1	+1.0	0.08	0.30	1.00		1.00
R	2	+1.8	0.66	0.53	1.00		1.00
P1	3	+2.5	0.95	0.72	(1.00)**		1.00
P1*$^{\|\|}$	3	+2.9	0.82	0.56	(1.00)**	0.91	1.00
F	1	+1.0	0.12	0.31	(1.00)**		1.00
O*$^{\#\#}$	0	−0.8	0.06	0.27	—		0.62

Average protonation of selected residues for different redox states of the binuclear center, with heme *a* and Cu_A considered oxidized. For the nomenclature of the different redox states and the charges on liganding oxygen species, see Fig. 1.

*Redox state of the binuclear center.

#Number of electrons on the binuclear site compared to the fully oxidized state.

§Change in net protonation, compared to the O state, calculated for the whole protein.

¶OH^- refers to the hydroxide ion bound to Cu_B.

||Calculation with His^{325} in its nonbound and thus protonatable orientation.

**The hydroxide ligand was not included in states with oxygen bound to the binuclear center.

##O* refers to the fully oxidized enzyme with no hydroxide/water bound to the binuclear site.

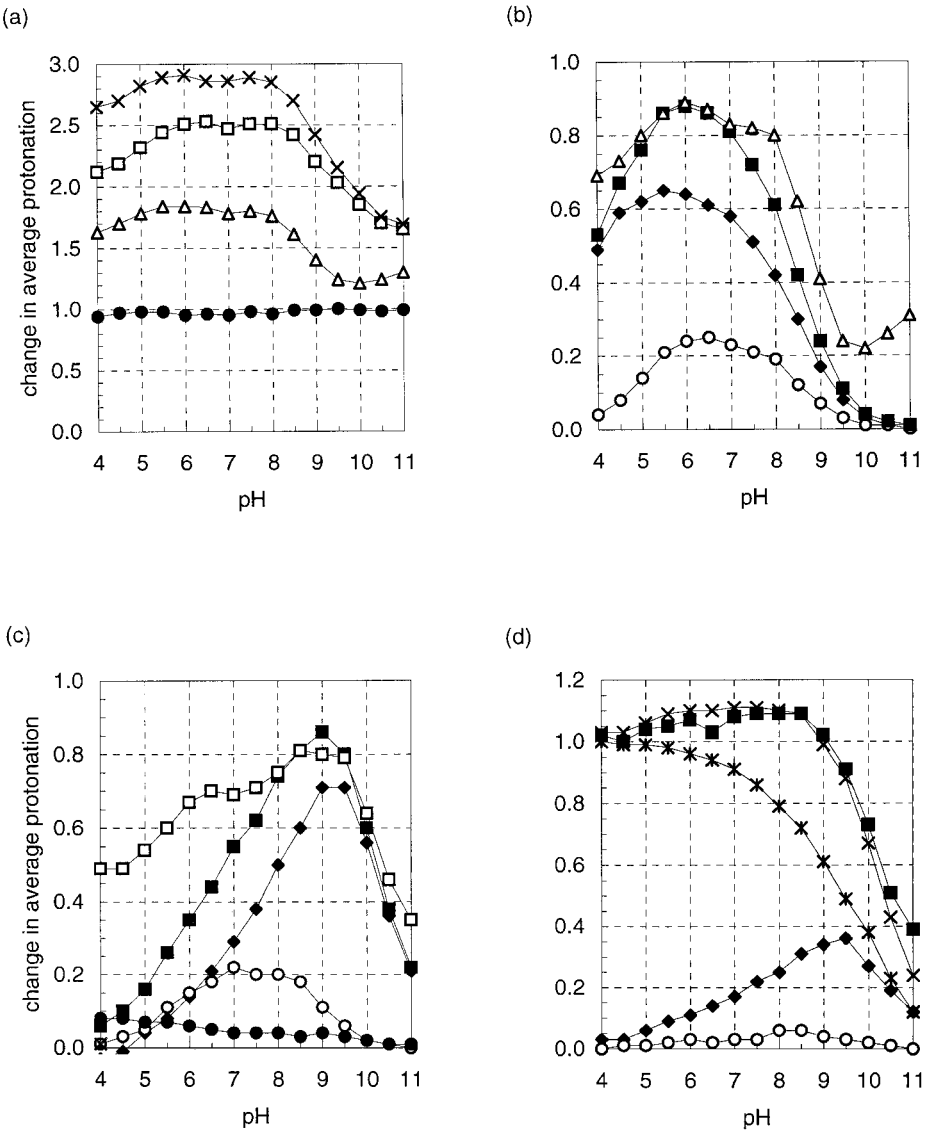

FIGURE 5 pH dependence of the change in net protonation associated with reduction of the binuclear center. (*a*) Change in net protonation calculated for the whole protein upon formation of the E state (●), R or A state (△), P1 state (□), and P1 state with His^{325} in its alternative orientation (×). (*b*) Change in average protonation associated with the E→R transition for $Glu^{II\text{-}78}$ (○), $Lys^{II\text{-}191}$ (♦), both residues (■), and the whole protein (△). (*c*) Changes associated with the A→P1 transition, His^{325} in its ligand bound orientation, for $Glu^{II\text{-}78}$ (○), $Lys^{II\text{-}191}$ (♦), Pra a_3 (●), the three residues together (■) and the whole protein (□). (*d*) Protonation changes for the A→P1 transition, His^{325} in its alternative orientation: $Glu^{II\text{-}78}$ (○), $Lys^{II\text{-}191}$ (♦), His^{325} (*), the three residues together (■) and the whole protein (×).

A (Chance et al., 1975). Electron transfer within the binuclear center leads to formation of the peroxy intermediate P, and subsequent electron input via Cu_A, and heme *a* then produces compound P1. The latter reaction is thermodynamically irreversible and traps the oxygen within the binuclear site (Verkhovsky et al., 1994). Recently Verkhovsky et al. (1996) have shown that it is the heme-to-heme transfer of the third electron that is essential for oxygen trapping to occur.

As its structure is yet unknown, the P state (Fig. 1) was not treated explicitly in our calculations. From the electrostatic point of view, it is very similar to the R and A states in that the charge at the binuclear center is the same. Control calculations yielded essentially the same results for the R and A states and a model of the P state as shown in Fig. 1.

As depicted in Fig. 2 *b*, the side chain of His^{325} was modeled in two different orientations: one is that of a Cu_B ligand, and the other one has the imidazole ring pointing away from the copper and forming hydrogen bonds with the formyl group of heme a_3, the hydroxyl group of Tyr^{328}, and the backbone carbonyl group of Phe^{340}. Conversion from the first to the second form could occur upon reduction of Cu_B and simultaneous stabilization of the nonbound histidine through protonation, as has been observed for the blue copper protein plastocyanin at low pH (Guss et al., 1986). Thus, starting from the E state (i.e., the one-electron reduced state with cuprous Cu_B), the alternative orientation of His^{325} was included in a parallel series of calculations. Its intrinsic pK was calculated as 4.4, arising from a desolvation penalty of 11.3 and a polar interaction energy of −9.1 ΔpK units. The latter is mainly due to the strong interaction with the heme a_3 formyl group (−4.6 ΔpK units) and the backbone carbonyl groups of residues 336–341 (together −4.7 ΔpK units). Nevertheless, in both the one-electron and the two-electron reduced enzyme, His^{325} was calculated to remain neutral between pH 4 and pH 11.5, and no significant differences in the protonation of other residues were found.

However, upon uptake of the third electron and transfer to the binuclear center, i.e., formation of the P1 state, His^{325} was calculated to become protonated (0.9 H^+ at pH 7.0), and thus the major contributor to a net proton uptake of 1.1 H^+, compared to the two-electron reduced state (cf. Table 2). With the histidine in its Cu_B-bound orientation, a net increase in protonation of 0.7 H^+ was calculated, with $Lys^{II\text{-}191}$ (+0.29 H^+), $Glu^{II\text{-}78}$ (+0.19 H^+) and the coupled groups Asp^{399}/Pra a_3 (+ 0.05 H^+) becoming more protonated. Thus, because reduction of heme *a* was calculated to be associated with the uptake of 0.8 H^+, the heme-heme electron transfer did not cause a significant change in net protonation.

After the reduction of oxygen and the formation of a water molecule, the oxoferryl or F state is formed. Electrostatically, it strongly resembles the E state, with the heme a_3 being reduced, and hence the protonation state of the enzyme was found to be very similar. The change in net protonation (compared to the O state) was calculated as +1.0 H^+, with the proton uptake being solely due to the hydroxide ion bound to the binuclear center.

To complete the reaction cycle, a fourth electron is transferred to the binuclear site (to form a redox state that is electrostatically similar to the R or A state of the enzyme), upon which the oxoferryl species is reduced and the binuclear site returns to its fully oxidized state. This might occur through a hydroxy intermediate H (Han et al., 1990; Fig. 1) with the hydroxide bound to the heme a_3 iron. The OH^- could then be transferred to Cu_B, restoring the O state of the enzyme.

The pH dependence of the net proton uptake by the enzyme upon reduction of the binuclear site is depicted in Fig. 5. It can be seen that the overall proton stochiometry is remarkably independent of pH, remaining at ± 0.2 H^+ of the average value between pH 4 and 9 (Fig. 5 *a*). Above pH 9, however, the number of accepted protons decreases dramatically. Up to the formation of the R state, the calculated change in net protonation over the whole range of pH is nearly exclusively due to proton uptake by $Lys^{II\text{-}191}$, $Glu^{II\text{-}78}$, and the hydroxide bound to Cu_B (Fig. 5 *b*). The former two residues also contribute to the net proton uptake upon formation of the P1 state (Fig. 5 *c*). However, if His^{325} in its nonbound orientation is included in the calculations, the bulk of the change in net protonation is due to His^{325} (Fig. 5 *d*).

Influence of the hydroxide ligand

We have seen that protonation of the hydroxide ion liganding Cu_B accounts for most of the change in net protonation calculated to occur upon partial reduction of the binuclear center. This raises the questions of how the hydroxide ion influences the average protonation of nearby residues in the fully oxidized state and whether the proton uptake upon electron transfer to the binuclear site can be accounted for by other residues when the hydroxide is not present. To address these questions, we have performed an additional series of calculations, omitting the hydroxide ion.

The ligand in its anionic form stabilizes the protonated states of nearby acidic and basic residues. Consequently, omitting the hydroxide caused the overall protonation of the protein to drop by 0.8 H^+. This is mainly due to proton release from Tyr^{280} (−0.38 H^+, cf. Table 2). In addition, $Glu^{II\text{-}78}$, $Lys^{II\text{-}191}$, Asp^{477}, and His^{85} were calculated to have lost between 0.03 and 0.07 H^+ each.

The finding of Tyr^{280} becoming partially deprotonated ($pK_a = 7.6$) is quite surprising, as all other tyrosine residues were determined to be neutral over the whole range of pH and for all redox states. Tyr^{280} strongly interacts with the binuclear site (−8.3 and −8.2 ΔpK units with heme a_3 and Cu_B, respectively). However, these interactions were partially compensated (+8.6 ΔpK units) when the hydroxide ligand was included, causing the Tyr^{280}, like all other tyrosines, to remain neutral. Thus there were no charge-charge interactions with other residues, and the pK_a was equal to pK_{int} (29.1).

When the hydroxide ligand had been included in the calculations, it was found to become fully protonated to water upon reduction of either heme a_3 or Cu_B. This also means, however, that charge-charge interactions with nearby residues are abolished. Thus, from the one-electron reduced state up to the regeneration of the O state upon which the catalytic cycle is completed, this water should have no influence on the average protonation of other residues and, indeed, no differences were found when the water was omitted. Upon formation of the E state, 0.8 H^+ were calculated to be taken up, with Tyr^{280} becoming fully protonated. Hence, with the exception of the O state, results shown in Table 2 are also valid for the case in which the water molecule was not included.

Influence of the membrane model

As described in the Methods section, we have introduced a membrane model to account for the low-dielectric environment at the parts of the molecular surface that are exposed to the hydrophobic regions of the membrane. Consequently, this resulted in a marked increase in desolvation penalty for residues exposed to or close to the now membrane-covered part of the surface. His^{464}, for example, is relatively close to the protein-solvent interface when no membrane model is used. Upon introduction of the membrane model, however, the residue becomes deeply buried within the low dielectric, and thus the desolvation penalty increases to 11.6 ΔpK units.

Without the membrane model, the isoelectric point of the protein complex was calculated as 4.7 for the two-subunit enzyme in its fully oxidized state, which is only marginally different from the value of 4.6 calculated for the enzyme with the membrane model. Sixteen residues of subunits I and II were found to change their average protonation by more than 0.1 H^+ at at least one pH value between 4 and 11.5 when the membrane model was omitted. A drastic change, for example, was calculated for Arg^{129}; its pK_a dropped by more than 5 ΔpK units from above 11.5 to 6.5.

The side chain of this residue is very close to the protein-solvent (or protein-membrane) interface; thus the decrease in pK_a arises from a desolvation penalty that is 5.8 ΔpK units lower without the membrane model. However, leaving out the membrane model did not significantly alter the stochiometry of the protonation changes that occur upon electron transfer. Residues that were calculated to change their protonation upon reduction of the cofactors were the same with or without the membrane model, and their individual changes in average protonation were not found to be significantly different.

As control calculations have shown, including subunits III and IV (Iwata et al., 1995) in the calculations did not lead to an increase in the number of sites that strongly interact with the cofactors; nor does it significantly affect the proton stochiometry and the sites that were calculated to be involved in proton uptake.

DISCUSSION

We have used a continuum dielectric model and finite-difference technique to analyze the electrostatic coupling between protonatable residues and cofactors of *P. denitrificans* cytochrome *c* oxidase. We have determined the average protonation of all titratable residues through Monte Carlo sampling and analyzed changes in protonation that occur upon reduction of the redox-active sites.

One of the main results of our study is the identification and characterization of a core of titratable residues that strongly electrostatically interact with the redox centers and account for most of the protonation changes coupled to electron transfer. Similar cores or clusters of interacting protonatable residues as the result of computational analyses have been reported for the photosynthetic reaction centers of *Rps. viridis* (Lancaster et al., 1996) and *Rb. sphaeroides* (Beroza et al., 1995; Gunner and Honig, 1992). However, using the same threshold criterion for "strong" interactions, the cluster determined for the *Rps. viridis* reaction center comprised 47 protonatable groups, compared to only 18 residues that strongly interact with the cofactors in cytochrome *c* oxidase. Plainly, this is due to the limited number of titratable residues within the transmembranous part of cytochrome *c* oxidase close enough to the cofactors or each other to build up such a large "network" of interacting residues.

The strong coupling of residues within such a core has consequences for the estimated error of the calculations. Whereas in isolated titration sites the region of fractional protonation is limited to a small pH range, it can be expected to extend over a wider range of the pH within a cluster of interacting residues. Thus it is easier to estimate the net protonation within this pH range, but it is more difficult to determine how this protonation is distributed over the coupled residues (Lancaster et al., 1996). Therefore, care must be taken in assigning protonation changes to individual groups within such a cluster, because even subtle conformational changes within the cluster may cause a redistribution of protons over the cluster without, however, affecting the net protonation of the cluster.

We have included a nonredox active magnesium ion in our calculations, the potential role of which in catalysis is still unclear. The calculations showed that, although the positive charge of the magnesium is effectively screened by the negative charges on the ligands Asp^{404} and $Glu^{II\text{-}218}$, it is important in defining the local electrostatics and thus in determining the distribution of protons among the residues of the core cluster. One could also speculate about its role in making Asp^{404} and $Glu^{II\text{-}218}$ effectively nonprotonatable, thereby preventing, for example, proton uptake from the periplasm.

According to our calculations, electron input into the enzyme is counterbalanced by an increase in net protonation by 0.7–1.1 H^+/e^-, two-electron reduction of the binuclear center being coupled to uptake of 1.8 H^+, and input of a third electron to either heme *a* or the binuclear site being associated with additional 0.7–1.1 H^+. These results are in good agreement with the experimentally determined values reported by Rich and co-workers for bovine heart cytochrome *c* oxidase (Mitchell et al., 1992; Mitchell and Rich, 1994; summarized in Rich et al., 1996). They showed that reduction of the enzyme is coupled to uptake of 2.4 H^+ in the pH range 7.2–8.5, two of which were associated with the binuclear center, and the remaining 0.4 H^+ with heme a/Cu_A, probably with the heme, as the E_m of Cu_A is pH-independent (Blair et al., 1986). Similar values, also for the bovine heart enzyme, were obtained by Hallén and Nilsson (1992), who determined 2.6 H^+ (pH 7) to be taken up upon reduction, and recently by Capitanio et al. (1997), who, at pH 7 observed uptake of 2.1 H^+ upon reduction, 0.7 of which they associated with heme *a*. Thus our computational results are within the error margins of the experimentally determined values.

The proton uptake was calculated to be relatively independent of the pH up to pH 8.5 (Fig. 5). This agrees well with the experimental results by Hallén and Nilsson (1992) and Mitchell and Rich (1994), who found only slight alterations in the value of proton uptake in the pH ranges 6–8.5 and 7.2–8.5, respectively. In contrast, Capitanio et al. (1997) observed a marked increase in proton uptake from ~1 H^+ at pH 6 to a maximum of 2.7 H^+ at pH 8.5.

Redox-coupled proton uptake was calculated to be mostly confined to residues close to the cofactor being reduced, hence stabilizing its less positively charged (i.e., reduced) state. This could be of importance for the control of the electron transfer process itself, because acceptance of an electron by a metal center within a low-dielectric environment is energetically very unfavorable and cannot be met sufficiently by redistribution of local charges. Thus the reduced state must to be further stabilized, either by delocalization of the electron (e.g., over a conjugated system such as the heme macrocycle) or by simultaneous uptake of a proton or other cation that binds close to the redox center (as outlined by Rich, 1996). Such a proton-controlled pro-

cess has been proposed by Verkhovsky et al. (1995) for the initial heme *a*–heme a_3 electron transfer reaction. They suggested that electron transfer, despite being very fast, is limited by the initially low midpoint potential of heme a_3. Protonation of a site near the binuclear center, however, then raises the midpoint potential of the heme and the reduced population is stabilized. Interestingly, it is the hydroxide ligand that we have calculated to become protonated upon partial reduction of the binuclear center and which thus appears a likely candidate for the titratable group suggested by Verkhovsky et al. Furthermore, upon becoming protonated to water, it can dissociate from the binuclear site, thereby making way for the oxygen to bind. It has also been shown by Ädelroth et al. (1995, 1996) and Hallén et al. (1994) that electron transfer to heme a_3 is coupled to protonation of a group close to the binuclear site, and it has been speculated that a hydroxide ligand to Cu_B could be the proton-binding group (Hallén et al., 1994).

Uptake of an additional proton, leading to the formation of the A-state (Fig. 1), was calculated to be accompanied by protonation of residues Lys^{II-191} and Glu^{II-78}. Hence these groups, with the likely exception of Glu^{II-78}, may provide the "proton trap" (Rich, 1995; Wikström et al., 1994) that accounts for charge compensation but is physically separated from the oxygen chemistry. However, it should again be stressed that, with the exception of cases such as the Cu_B-bound hydroxide ion, which was calculated to take up 1 H^+ at all pH values upon partial reduction of the binuclear site, the assignment of the protonation change to individual sites within the strongly interacting cluster is problematic. Slightly differing sets of coordinates, e.g., from different states of the structural refinement, will yield different proton uptake profiles for some residues within the cluster without, however, affecting its net protonation (when using a slightly lower-resolution set of coordinates, for example, we calculated the coupled groups Asp^{399}/Pra a_3 to become protonated instead of Lys^{II-191}).

The finding that Glu^{II-78} changes its protonation state upon electron transfer to the binuclear center is quite surprising, as the residue is located some 25 Å away from the binuclear site (Fig. 6). Its titration curve was calculated to be relatively steep between pH 4.5 (92% protonation) and pH 8.5 (8% protonation). Thus, even a small shift in pK could give rise to a significant change in average protonation. In the case of Glu^{II-78}, this change in protonation was a result of direct interactions with heme a_3 (0.65 ΔpK units) and Cu_B (0.55 ΔpK units) and not propagated by changes in protonation of intervening residues. (The only strong inter-

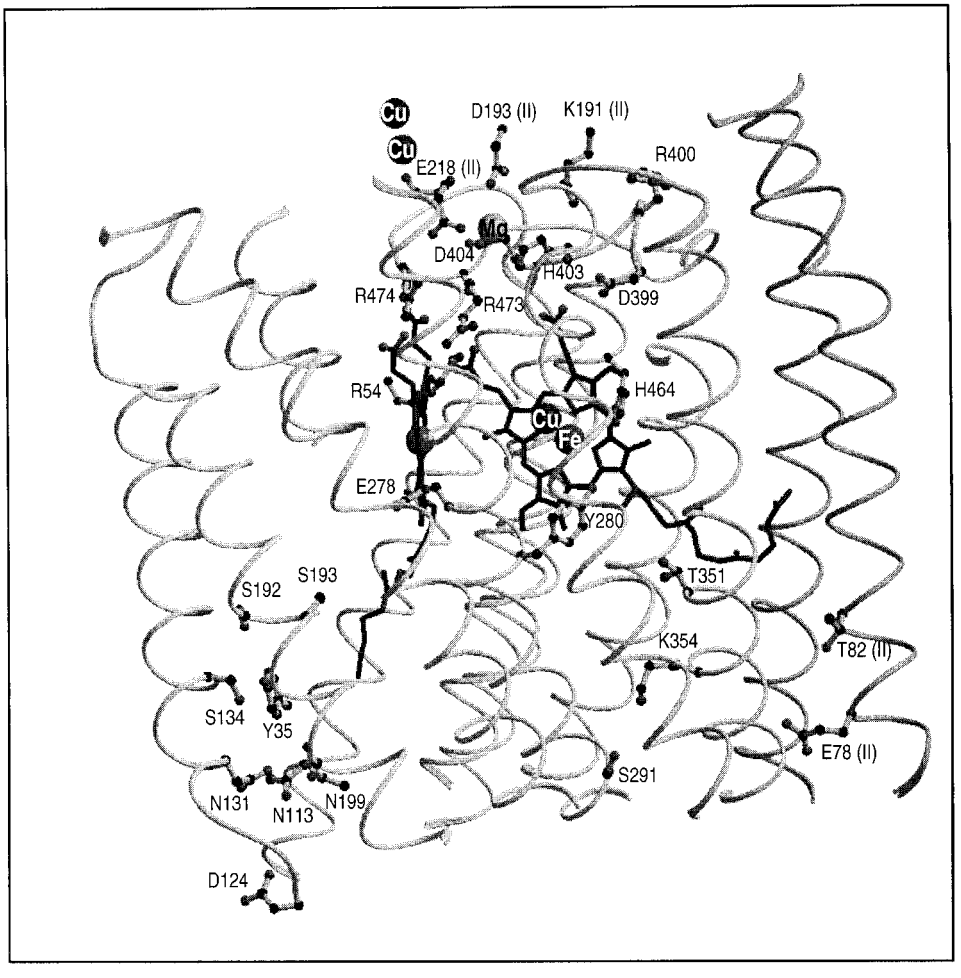

FIGURE 6 The core cluster of residues strongly interacting with the cofactors (see also Table 1). Additionally, the "isolated" sites Asp^{124} and Glu^{II-78}, and the conserved Thr^{II-82} are shown, and the residues providing the two putative proton channels (Iwata et al., 1995) are included. The figure was produced with MolScript and Raster3D.

action with a potentially charged group was that with Lys^{354} (2.6 ΔpK units), which, however, was calculated to be neutral in all redox states.) However, as for such an apparently electrostatically isolated site, the average protonation is very sensitive to changes in, for example, desolvation energy or polar interactions, the actual value of the proton uptake is difficult to assess. Nevertheless, such isolated groups close to the cytoplasmic side may be crucial as possible proton entry sites, because they can respond to electronic changes despite being very far away from the redox centers. Asp^{124}, for example, is such a group and has been shown to be a key residue for proton pumping (Thomas et al., 1993; Garcia-Horsman et al., 1995; see below). $Glu^{II\text{-}78}$, like Asp^{124}, is conserved among terminal heme-copper oxidases, and its location within the membrane is comparable to that of the aspartate (cf. Fig. 6). Thus it may be of importance for controlling the proton uptake, possibly through interactions with the so-called K-channel (see below) via the also conserved $Thr^{II\text{-}82}$.

An additional matter of debate is the nature of the "switch" that couples reduction of the oxygen to proton translocation, but at the same time prevents proton backflow into the cytoplasm. Within the framework of the histidine-cycle concept (Wikström et al., 1994), His^{325}, cycling between two different orientations, has been suggested to provide this "switch," by moving away from Cu_B and becoming doubly protonated, with its positive charge stabilized electrostatically by the electrons taken up by the binuclear center (Iwata et al., 1995). The results of our calculations are in general agreement with this proposal. However, as we have calculated His^{325} to become doubly protonated only upon formation of the P1 state, they differ from the model suggested by Iwata et al. (1995), in which the histidine moves away from the copper already upon reduction of the binuclear site.

Proton transfer pathways

In the crystal structure of the *P. denitrificans* cytochrome *c* oxidase, two possible proton pathways have been identified (Iwata et al., 1995). The shorter one, which is also referred to as the K-pathway, leads to the binuclear site via the highly conserved residues Lys^{354}, Thr^{351}, and Tyr^{280}, and has been discussed as the pathway for "chemical" protons that are required for water formation. The second, longer pathway (D-pathway) involves, in addition to a number of polar residues, the two titratable residues Asp^{124} and Glu^{278}, which are also highly conserved among terminal heme-copper oxidases. On the grounds of site-directed mutagenesis studies (Thomas et al., 1993; Garcia-Horsman et al., 1995), in which the mutation of the aspartate to an asparagine led to an enzyme that, although incapable of proton pumping, was still able to reduce oxygen (albeit with a lower activity), the D-pathway has been proposed as the pathway for the "pumped" protons.

From the characterization of other site-directed mutants (Konstantinov et al., 1997; Vygodina et al., 1996; Hosler et al., 1996; Svensson-Ek et al., 1996; Verkhovskaya et al., 1997) it now seems to be clear that the three protonatable amino acids Lys^{354}, Asp^{124}, and Glu^{278} are indeed key residues for proton transfer to the binuclear center. Interestingly, charge translocation studies (Konstantinov et al., 1997) and the finding that mutation of Lys^{354} inhibits reduction of heme a_3 (Hosler et al., 1996) suggest that the lysine and hence the K-pathway are of importance only for the eu-oxidase part of the catalytic cycle, i.e., the O→R transitions but do not seem to be crucial for the P→O part of the cycle. On the other hand, mutation of the D-pathway residues was found to completely abolish proton translocation associated with the peroxidase part, i.e., the P→O transition. Thus the two pathways seem to be important for different halves of the catalytic cycle rather than for chemical or pumped protons. One could speculate that the bound oxygen molecule blocks further proton uptake along the K-pathway, e.g., through interactions with Tyr^{280}. Alternatively, blocking of the pathway may occur through subtle conformational changes in the binuclear center caused by reduction and/or the associated protonation.

In this study, both Glu^{278} and Lys^{354} were calculated to be neutral at pH 7.0 for all redox states considered. This is mainly a result of the high degree of desolvation and the resulting loss of reaction field energy that is not compensated for by polar or charge-charge interactions. Furthermore, the side chains of both residues point into large cavities that might contain ordered solvent molecules. In our calculations, such water-filled cavities were treated as a high-dielectric continuum. However, as the charge-stabilizing effect of highly directed hydrogen bonds cannot be accounted for (see Methods section), this approach consequently yields higher pK_a values for acidic and lower pK_a values for basic residues (Yang et al., 1993).

Furthermore, protonation changes due to proton transfer are transient, i.e., residues that participate in proton transfer are not necessarily differently protonated in different equilibrium states. As part of a "proton wire," for example, the residue considered could well donate a proton to stabilize the reduced state of a cofactor. However, if the pK_a of the residue is high enough, this would be followed immediately by proton uptake either from other residues or from the solvent, so that there is no change in average protonation. Hence the results of our (equilibrium) calculations are not necessarily inconsistent with both Glu^{278} and Lys^{354} having a key role in proton transfer to the binuclear center. In fact, recent Fourier transform infrared spectroscopy studies indicate that Glu^{278} is protonated in the reduced enzyme (Puustinen et al., 1997) and might also be so in the oxidized state (Lübben and Gerwert, 1996). It has also been suggested by Puustinen et al. (1997) that a conformational change may be required for Glu^{278} to take part in proton transfer, which cannot be accounted for in our static computational model.

Other, more general sources of error are the accuracy of the surfacing algorithm and the quality of the structure, i.e., the potential error of the coordinates used for the calcula-

tions. In some cases, long amino acid side chains are poorly defined in the electron density map at the present level of resolution. Moreover, structural refinement was done without assigning partial charges, and thus the actual positions of protonatable groups are in some cases not very well defined. However, even small differences in the position of single amino acid side chains can have a great influence on the outcome of the computational analysis, as discussed by Lancaster et al. (1996) for the bacterial reaction center. Hence, higher resolution structural information will be needed to further improve the reliability of the computational analysis and to assess the significance of the results reported here.

CONCLUSION

Electrostatic calculations provide a valuable tool to analyze the response of titratable residues to changes in redox state. The work presented in this study can help to elucidate how electron transfer in cytochrome *c* oxidase is coupled to proton translocation, and which particular residues possibly contribute to protonation changes associated with reduction of cofactors.

We have characterized a cluster of strongly interacting titratable groups that accounts for most of the protonation changes linked to electron transfer. The overall stoichiometry of these protonation changes is in good agreement with reported experimental values. Special consideration has been given to the groups that were calculated to accept or release protons upon reduction of the binuclear center. A hydroxide ligand to Cu_B was calculated to become protonated to water upon electron transfer to the binuclear site and could thus be important in both triggering heme-heme electron transfer and allowing oxygen binding. Within the limits of the computational model and the available structural information, results presented here can be useful for the design of new experiments to further evaluate the mechanism of coupling of electron transfer and proton translocation and the role of individual amino acid residues within this complex process.

We are grateful to Marilyn R. Gunner for the use of her computer programs and Anthony Nicholls and Barry Honig for modifications of DelPhi. We thank Mårten Wikström, Julia Behr, and Axel Harrenga for valuable discussions.

AK gratefully acknowledges financial support from the Fond der Chemischen Industrie.

REFERENCES

Ädelroth, P., P. Brzezinski, and B. G. Malmström. 1995. Internal electron transfer in cytochrome *c* oxidase from *Rhodobacter sphaeroides*. *Biochemistry.* 34:2844–2849.

Ädelroth, P., H. Sigurdson, S. Hallén, and P. Brzezinski. 1996. Kinetic coupling between electron and proton transfer in cytochrome *c* oxidase: simultaneous measurements of flash-induced absorbance and conductance changes. *Proc. Natl. Acad. Sci. USA.* 93:12292–12297.

Babcock, G. T., and M. Wikström. 1992. Oxygen activation and the conservation of energy in cell respiration. *Nature.* 356:301–309.

Bacon, D. J., and W. F. Anderson. 1988. A fast algorithm for rendering space-filling molecule pictures. *J. Mol. Graphics.* 6:219–220.

Bashford, D., and K. Gerwert. 1992. Electrostatic calculations of the pK_a values of ionizable groups in bacteriorhodopsin. *J. Mol. Biol.* 224: 473–486.

Beroza, P., D. R. Fredkin, M. Y. Okamura, and G. Feher. 1991. Protonation of interacting residues in a protein by a Monte Carlo method: application to lysozyme and the photosynthetic reaction center of *Rhodobacter sphaeroides*. *Proc. Natl. Acad. Sci. USA.* 88:5804–5808.

Beroza, P., D. R. Fredkin, M. Y. Okamura, and G. Feher. 1995. Electrostatic calculations of amino acid titration and electron transfer, $Q_A^- Q_B \rightarrow Q_A Q_B^-$, in the reaction center. *Biophys. J.* 68:2233–2250.

Blair, D. F., W. R. Ellis, Jr., H. Wang, H. B. Gray, and S. I. Chan. 1986. Spectroelectrochemical study of cytochrome *c* oxidase: pH and temperature dependences of the cytochrome potentials. *J. Biol. Chem.* 216: 11524–11537.

Brooks, B. R., R. E. Bruccoleri, B. D. Olafson, D. J. States, S. Swaminathan, and M. Karplus. 1983. CHARMM: a program for macromolecular energy minimization and dynamics calculations. *J. Comp. Chem.* 4:187–217.

Capitanio, N., T. V. Vygodina, G. Capitanio, A. A. Konstantinov, P. Nicholls, and S. Papa. 1997. Redox-linked protolytic reactions in soluble cytochrome *c* oxidase from beef-heart mitochondria: redox Bohr effects. *Biochim. Biophys. Acta.* 1318:255–265.

Chance, B., C. Saronio, and J. S. Leigh. 1975. Functional intermediates in the reaction of membrane-bound cytochrome oxidase with oxygen. *J. Biol. Chem.* 250:9226–9237.

Condon, P. J., and W. E. Royer, Jr. 1994. Crystal structure of oxygenated Scapharca dimeric hemoglobin at 1.7 Å resolution. *J. Biol. Chem.* 269:25259–25267.

Connolly, M. L. 1983. Analytical molecular surface calculation. *J. Appl. Crystallogr.* 16:548–558.

Fann, Y. C., I. Ahmed, N. J. Blackburn, J. S. Boswell, M. L. Verkhovskaya, B. M. Hoffman, and M. Wikström. 1995. Structure of Cu_B in the binuclear heme-copper center of the cytochrome aa_3-type quinol oxidase from *Bacillus subtilis*: an ENDOR and EXAFS study. *Biochemistry.* 34:10245–10255.

Fetter, J. R., J. Quian, J. Shapleigh, J. W. Thomas, J. A. Garcia-Horsman, E. Schmidt, J. Hosler, G. T. Babcock, R. B. Gennis, and S. Ferguson-Miller. 1995. Possible proton relay pathways in cytochrome *c* oxidase. *Proc. Natl. Acad. Sci. USA.* 92:1604–1608.

Garcia-Horsman, J. A., A. Puustinen, R. B. Gennis, and M. Wikström. 1995. Proton transfer in cytochrome bo_3 ubiquinol oxidase of *Escherichia coli*: second-site mutations in subunit I that restore proton pumping in the mutant Asp-135 → Asn. *Biochemistry.* 34:4428–4433.

Gilson, M. K., K. A. Sharp, and B. Honig. 1987. Calculating the electrostatic potential of molecules in solution: method and error assessment. *J. Comp. Chem.* 9:327–335.

Gunner, M. R., and B. Honig. 1992. Calculations of proton uptake in *Rhodobacter sphaeroides* reaction centers. *In* The Photosynthetic Bacterial Reaction Center, Vol. II. J. Breton and A. Vermeglio, editors. Plenum Press, New York.

Guss, J. M., P. R. Haarowell, M. Murata, V. A. Norris, and H. C. Freeman. 1986. Crystal structure analyzes of reduced (Cu I) plastocyanin at six pH values. *J. Mol. Biol.* 192:361–387.

Hallén, S., P. Brzezinski, and B. G. Malmström. 1994. Internal electron transfer in cytochrome *c* oxidase is coupled to the protonation of a group close to the bimetallic site. *Biochemistry.* 33:1467–1472.

Hallén, S., and T. Nilsson. 1992. Proton transfer during the reaction between fully reduced cytochrome *c* oxidase and dioxygen: pH and deuterium isotope effects. *Biochemistry.* 31:11853–11859.

Haltia, T., M. Saraste, and M. Wikström. 1989. Subunit III of cytochrome *c* oxidase is not involved in proton translocation: a site-directed mutagenesis study. *EMBO J.* 10:2015–2021.

Han, S., Y. Ching, and D. L. Rousseau. 1990. Ferryl and hydroxy intermediates in the reaction of oxygen with reduced cytochrome *c* oxidase. *Nature.* 348:89–90.

Hendler, R. W., K. Pardhasaradhi, B. Reynafarje, and B. Ludwig. 1991. Comparison of energy-transducing capabilities of the two- and three-

subunit cytochromes aa_3 from *Paracoccus denitrificans* and the 13-subunit beef heart enzyme. *Biophys. J.* 60:415–423.

Hosler, J. P., J. P. Shapleigh, D. M. Mitchell, Y. Kim, M. A. Pressler, C. Georgiou, G. T. Babcock, J. O. Alben, S. Fergusson-Miller, and R. B. Gennis. 1996. Polar residues in helix VIII of subunit I of cytochrome *c* oxidase influence the activity and the structure of the active site. *Biochemistry.* 35:10776–10783.

Iwata, S., C. Ostermeier, B. Ludwig, and H. Michel. 1995. Structure at 2.8 Å resolution of cytochrome *c* oxidase from *Paracoccus denitrificans. Nature.* 376:660–669.

Konstantinov, A. A., S. Siletsky, D. Mitchell, A. Kaulen, and R. B. Gennis. 1997. The roles of the two proton input channels in cytochrome *c* oxidase from *Rhodobacter sphaeroides* probed by the effects of site-directed mutations on time-resolved electrogenic intraprotein proton transfer. *Proc. Natl. Acad. Sci. USA.* 94:9085–9090.

Kraulis, P. J. 1991. MolScript, a program to produce both detailed and schematic plots of protein structures. *J. Appl. Crystallogr.* 24:946–950.

Lancaster, C. R. D. 1996. The coupling of light-induced electron transfer and proton uptake in the photosynthetic reaction centre from *Rhodopseudomonas viridis*. Ph.D. thesis. University of Frankfurt am Main.

Lancaster, C. R. D., H. Michel, B. Honig, and M. R. Gunner. 1996. Calculated coupling of electron and proton transfer in the photosynthetic reaction center of *Rhodopseudomonas viridis*. *Biophys. J.* 70: 2469–2492.

Lübben, M., and K. Gerwert. 1996. Redox FTIR difference spectroscopy using caged electrons reveals contributions of carboxyl groups to the catalytic mechanism of haem-copper oxidases. *FEBS Lett.* 397:303–307.

Merritt, E. A., and M. E. P. Murphy. 1994. Raster3D version 2.0—a program for photorealistic molecular graphics. *Acta Crystallogr.* D50: 869–873.

Mitchell, R., P. Mitchell, and P. R. Rich. 1992. Protonation states of the catalytic intermediates of cytochrome *c* oxidase. *Biochim. Biophys. Acta.* 1101:188–191.

Mitchell, R., and P. R. Rich. 1994. Proton uptake by cytochrome *c* oxidase on reduction and on ligand binding. *Biochim. Biophys. Acta.* 1186: 19–26.

Nicholls, P. 1974. On the nature of cytochrome a_3. *In* Dynamics of Energy-Transducing Membranes. L. Ernster, R. W. Estabrook, and E. C. Slater, editors. Elsevier, Amsterdam. 39–50.

Nicholls, A., and B. Honig. 1991. A rapid finite difference algorithm, utilizing successive over-relaxation to solve the Poisson-Boltzmann equation. *J. Comp. Chem.* 12:435–445.

Nicholls, A., K. A. Sharp, and B. Honig. 1991. Protein folding and association: insights from the interfacial and thermodynamic properties of hydrocarbons. *Proteins.* 11:281–296.

Ostermeier, C., A. Harrenga, U. Ermler, and H. Michel. 1997. Structure at 2.7 Å resolution of the *Paracoccus denitrificans* two-subunit cytochrome *c* oxidase complexed with an antibody F_V fragment. *Proc. Natl. Acad. Sci. USA.* 94:10547–10553.

Puustinen, A., J. A. Bailey, R. B. Dyer, S. L. Mecklenburg, M. Wikström, and W. H. Woodruff. 1997. Fourier transform infrared evidence for connectivity between Cu_B and glutamic acid 286 in cytochrome bo_3 from *E. coli. Biochemistry.* 36:13195–13200.

Rich, P. R. 1995. Towards an understanding of the chemistry of oxygen reduction and proton translocation in the iron-copper respiratory oxidases. *Aust. J. Plant Physiol.* 22:479–486.

Rich, P. R. 1996. Electron transfer complexes coupled to ion translocation. *In* D. S. Bendall, editor. Protein Electron Transfer. Bios Scientific Publishers, Oxford. 217–242.

Rich, P. R., B. Meunier, R. Mitchell, and A. J. Moody. 1996. Coupling of charge and proton movement in cytochrome *c* oxidase. *Biochim. Biophys. Acta.* 1275:91–95.

Rousseau, D. L., Y.-C. Ching, and J. Wang. 1993. Proton translocation in cytochrome *c* oxidase: redox linkage through proximal ligand exchange on cytochrome a_3. *J. Bioenerg. Biomembr.* 25:165–177.

Sudmeier, J. L., and C. N. Reilley. 1964. Nuclear magnetic resonance studies of protonation of polyamine and aminocarboxylate compounds in aqueous solution. *Anal. Chem.* 36:1699–1706.

Svensson-Ek, M., J. W. Thomas, R. B. Gennis, T. Nilsson, and P. Brzezinski. 1996. Kinetics of electron and proton transfer during the reaction of wild type and helix VI mutants of cytochrome bo_3 with oxygen. *Biochemistry.* 35:13673–13680.

Tanford, C., and J. G. Kirkwood. 1957. Theory of protein titration curves. I. General equations for impenetrable spheres. *J. Am. Chem. Soc.* 79: 5333–5339.

Thomas, J. W., A. Puustinen, J. O. Alben, R. B. Gennis, and M. Wikström. 1993. Substitution of asparagine for aspartate-135 in subunit I of the cytochrome *bo* ubiquinol oxidase of *Escherichia coli* eliminates proton-pumping activity. *Biochemistry.* 32:10923–10928.

Tsukihara, T., H. Aoyama, E. Yamashita, T. Tomizaki, H. Yamaguchi, K. Shinzawa-Itoh, R. Nakashima, R. Yaono, and S. Yoshikawa. 1995. Structures of metal sites of oxidized bovine heart cytochrome *c* oxidase at 2.8 Å. *Science.* 269:1069–1074.

Tsukihara, T., H. Aoyama, E. Yamashita, T. Tomizaki, H. Yamaguchi, K. Shinzawa-Itoh, R. Nakashima, R. Yaono, and S. Yoshikawa. 1996. The whole structure of the 13-subunit oxidized cytochrome *c* oxidase at 2.8 Å. *Science.* 272:1136–1144.

Varotsis, C., and G. T. Babcock. 1990. Appearance of the $\nu(Fe^{IV} = 0)$ vibration from a ferryl-oxo intermediate in the cytochrome oxidase/dioxygen reaction. *Biochemistry.* 29:7357–7362.

Verkhovskaya, M. L., A. Garcia-Horsman, A. Puustinen, J.-L. Rigaud, J. E. Morgan, M. I. Verkhovsky, and M. Wikström. 1997. Glutamic acid 286 in subunit I of cytochrome bo_3 is involved in proton translocation. *Proc. Natl. Acad. Sci. USA.* 94:10128–10131.

Verkhovsky, M. I., J. E. Morgan, A. Puustinen, and M. Wikström. 1996. Kinetic trapping of oxygen in cell respiration. *Nature.* 380:268–270.

Verkhovsky, M. I., J. E. Morgan, M. L. Verkhovskaya, and M. Wikström. 1997. Translocation of electrical charge during a single turnover of cytochrome *c* oxidase. *Biochim. Biophys. Acta.* 1318:6–10.

Verkhovsky, M. I., J. E. Morgan, and M. Wikström. 1994. Oxygen binding and activation: early steps in the reaction of oxygen with cytochrome *c* oxidase. *Biochemistry.* 33:3079–3086.

Verkhovsky, M. I., J. E. Morgan, and M. Wikström. 1995. Control of electron delivery to the oxygen reduction site of cytochrome *c* oxidase: a role for protons. *Biochemistry.* 34:7483–7491.

Vygodina, T., D. Mitchell, C. Pecoraro, R. B. Gennis, and A. A. Konstantinov. 1996. Effect of amino acid replacements in the two proton channels of *Rh. sphaeroides* cytochrome *c* oxidase on the reaction of the enzyme with H_2O_2. EBEC reports. *Biochim. Biophys. Acta.* 9:B-32.

Wikström, M. 1989. Identification of the electron transfers in cytochrome oxidase that are coupled to proton pumping. *Nature.* 338:776–778.

Wikström, M., A. Bogachev, M. Finel, J. E. Morgan, A. Puustinen, M. Raitio, M. L. Verkhovskaya, and M. I. Verkhovsky. 1994. Mechanism of proton translocation by the respiratory oxidases. The histidine cycle. *Biochim. Biophys. Acta.* 1187:106–111.

Wikström, M., H. J. Harmon, W. J. Ingledew, and B. Chance. 1976. A re-evaluation of the spectral, potentiometric and energy-linked properties of cytochrome *c* oxidase in mitochondria. *FEBS Lett.* 65:259–277.

Wilson, D. F., J. G. Lindsay, and E. S. Brocklehurst. 1972. Heme-heme interactions in cytochrome oxidase. *Biochim. Biophys. Acta.* 256: 277–286.

Woodruff, W. H. 1993. Coordination dynamics of heme-copper oxidases. The ligand shuttle and the control and coupling of electron transfer and proton translocation. *J. Bioenerg. Biomembr.* 25:177–188.

Yang, A.-S., M. R. Gunner, R. Sampogna, K. Sharp, and B. Honig. 1993. On the calculation of pK_as in proteins. *Proteins.* 15:252–265.